

# Strong system-bath coupling reshapes characteristics of quantum thermal machines

Felix Ivander,<sup>1,\*</sup> Nicholas Anto-Sztrikacs,<sup>2,\*</sup> and Dvira Segal<sup>1,2</sup>

<sup>1</sup>*Chemical Physics Theory Group, Department of Chemistry and Centre for Quantum Information and Quantum Control, University of Toronto, 80 Saint George St., Toronto, Ontario, M5S 3H6, Canada*

<sup>2</sup>*Department of Physics, 60 Saint George St., University of Toronto, Toronto, Ontario, Canada M5S 1A7*  
(Dated: November 10, 2021)

We study the performance of quantum absorption refrigerators, paradigmatic autonomous quantum thermal machines, and reveal central impacts of strong couplings between the working system and the thermal baths. Using the reaction coordinate quantum master equation method, which treats system-bath interactions beyond weak coupling, we discover that *reshaping* of the window of performance is a central outcome of strong system-bath couplings. This alteration of the cooling window stems from the dominant role of parameter renormalization at strong couplings. We further show that strong coupling admits direct transport pathways between the thermal reservoirs. Such beyond-second-order transport mechanisms are typically detrimental to the performance of quantum thermal machines. Our study reveals that it is inadequate to claim for either a suppression or an enhancement of the cooling performance at strong coupling—when analyzed against a single parameter and in a limited domain. Rather, a comprehensive approach should be adopted so as to uncover the reshaping of the operation window.

*Introduction.*— The development of classical thermodynamics during the 19th century was directly tied to its application in building macroscopic heat engines. Fast forward to present times, the field of quantum thermodynamics [1–3] is similarly advanced by analyzing concrete machines such as the quantum Otto cycle or quantum absorption refrigerators. An early theoretical exploration of a small-scale quantum device was done by Scovil and Schulz-DuBois [4] who showed that a 3-level system could operate as a heat engine (maser). Nowadays, miniaturized thermal machines are experimentally realized from systems as small as a few trapped ions [5], a single atom [6], and electron spins [7]. Quantum thermal machines are distinct from their classical counterparts by relying on nonclassical effects such as quantum coherences [8–12], correlations [13, 14], measurements [14–16] and statistics [17], which may serve as a resource to enhance their performance beyond their classical analogues; studies cited here are representative of a growing literature.

Though not inherently a quantum mechanical effect, strong system-reservoir interactions are a common characteristic of quantum thermal devices due to the typical small scale of these machines and the fact that phase-coherent dynamics retains boundary effects. What is the impact of strong system-bath coupling on the performance of quantum thermal machines? Can we harness strong couplings to realize regimes of operation that are inaccessible at weak coupling? These questions were examined in different models, bringing model-dependent, sometimes conflicting answers [18–32]. On the one hand, strong system-bath coupling may open transport pathways that are inaccessible at weak coupling (e.g. by admitting high order processes and cooperative effects) [22, 24]. On the other hand, strong coupling between a system and its environment can suppress currents due to particle-dressing (polaron) physics [24, 33, 34].

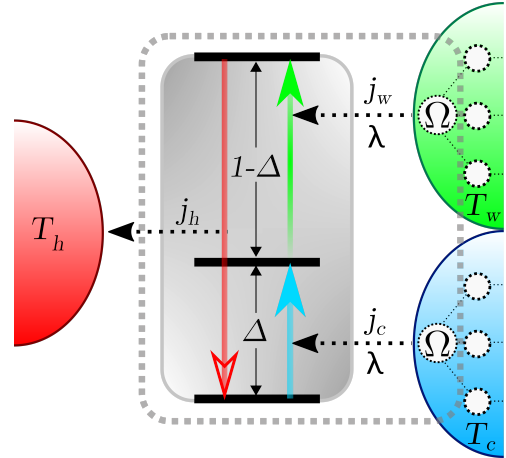


FIG. 1. Scheme of a 3-level QAR as investigated in this study. The thick blue, green and red arrows represent transitions induced by the cold, work and hot baths, respectively, exemplifying a cooling process. The dashed line (...) that encircles the system and part of the baths represents the repartitioning of the system and environment with the incorporation of collective bath coordinates into the system.

In this work, our goal is to provide a deep understanding over the impact of strong system-bath coupling on the performance of continuous-autonomous thermal machines, specifically, the paradigmatic 3-level model of a quantum absorption refrigerator (QAR) [4, 35–37]. This thermal machine extracts heat from a cold reservoir and transfers it to a hot bath by utilizing heat absorbed from an even hotter, “work” reservoir. QARs can be constructed from a single qubit [22], interacting qubits [38, 39], or multi-level quantum systems [10]. In this study, we concentrate on the 3-level model of QARs [35, 38, 39], depicted in Fig. 1. Recent studies examined different aspects of this machine, such as the impact

of dissipation and current leaks [36, 40], the role of internal coherences [10], current fluctuations [41, 42], and topology [43]. Furthermore, experimental implementations have been proposed [44] and realized [5]. While the question over the impact of strong system-bath coupling on the performance of QARs has been examined in different studies [18, 19, 22, 24], these sporadic results do not allow a comprehensive understanding. Is strong system-bath coupling beneficial or detrimental to the cooling operation of QARs?

Here, we reveal that a prominent impact of strong system-bath coupling in quantum thermal machines is the *reshaping* of the window of operation due to parameter renormalization. Watching the cooling current in a limited region may lead to conflicting conclusions as to whether it is enhanced or suppressed at strong coupling. In contrast, by using the powerful—and economic—reaction coordinate (RC) quantum master equation (QME) technique, which captures system-bath interactions beyond the weak coupling regime [34, 45–53], we observe the alteration of the performance window due to strong coupling. Besides reshaping the cooling window, we show that strong coupling opens direct bath-to-bath transport pathways, typically detrimental for the performance of quantum thermal machines.

*Model.*— A quantum absorption refrigerator cools an environment (temperature  $T_c$ ) by transferring its heat into a hot reservoir ( $T_h$ ). This is achieved with an energy input from a “work” bath ( $T_w$ ), where  $T_c < T_h < T_w$ . The process is mediated by a three-level system ( $i = 1, 2, 3$ ) playing the role of the classical working fluid. Transitions between energy levels of the quantum system are induced by the different reservoirs, see Fig. 1. The Hamiltonian describing this setup is given by

$$\hat{H}_{QAR} = \sum_{i=1}^3 \epsilon_i |i\rangle \langle i| + \sum_{\alpha=\{c,w,h\}} \sum_k \nu_{\alpha,k} \left( \hat{c}_{\alpha,k}^\dagger + \hat{S}_\alpha \frac{f_{\alpha,k}}{\nu_{\alpha,k}} \right) \left( \hat{c}_{\alpha,k} + \hat{S}_\alpha \frac{f_{\alpha,k}}{\nu_{\alpha,k}} \right). \quad (1)$$

Here,  $\epsilon_i$  denotes the energy of the  $i$ th level of the QAR. In what follows and without loss of generality, we set the total energy gap as  $\epsilon_3 - \epsilon_1 = 1$ , and define the first gap by  $\Delta \equiv \epsilon_2 - \epsilon_1$ . As for the baths,  $\hat{c}_{\alpha,k}^\dagger$  ( $\hat{c}_{\alpha,k}$ ) are bosonic creation (annihilation) operators of the  $\alpha = c, h, w$  reservoir for a mode of frequency  $\nu_{\alpha,k}$ . The baths’ harmonic oscillators couple to different transitions in the system with strength  $f_{\alpha,k}$ , assumed a real number. The system operators  $\hat{S}_\alpha$  couple to the different baths. The effects of these interactions are captured by the spectral density functions,  $J_\alpha(\omega) = \sum_k f_{\alpha,k}^2 \delta(\omega - \nu_{\alpha,k})$ . Setting the allowed transitions as  $\hat{S}_c = |1\rangle \langle 2| + \text{h.c.}$ ,  $\hat{S}_h = |1\rangle \langle 3| + \text{h.c.}$ ,  $\hat{S}_w = |2\rangle \langle 3| + \text{h.c.}$  allows for the maximal (Carnot) efficiency to be reached at weak coupling at a certain point [10, 35, 36]. For reasons explained shortly, the spectral

density function is chosen to be a peaked Brownian oscillator function for the cold and work baths ( $\alpha = w, c$ ),

$$J_\alpha(\omega) = \frac{4\omega\gamma_\alpha\Omega_\alpha^2\lambda_\alpha^2}{(\omega^2 - \Omega_\alpha^2)^2 + (2\pi\gamma_\alpha\Omega_\alpha\omega)^2}. \quad (2)$$

Here,  $\lambda_\alpha$  captures the system-environment coupling strength, and it is the central parameter of this work.  $\gamma_\alpha$  is a measure of the width of the spectral function, and  $\Omega_\alpha$  is the frequency about which the spectral density is peaked. To contrast, the hot bath spectral density is chosen to be an Ohmic function

$$J_h(\omega) = \gamma_h\omega e^{-|\omega|/\Lambda_h}, \quad (3)$$

with  $\gamma_h$  dictating the coupling strength between the hot bath and the QAR and  $\Lambda_h$  a high frequency cutoff.

*Reaction coordinate mapping.*— To go beyond a weak coupling treatment, we extract collective modes (“reaction coordinates”) from the heat baths and include them within the system’s Hamiltonian, to redefine the system-environment boundary. For computational efficiency, we assume that the system is weakly coupled to the hot ( $h$ ) bath, while allowing arbitrary coupling to the cold and work baths. We thus extract two RCs, from the cold and work baths, each. It is straightforward to further include a collective mode from the hot bath. This exact mapping results in the following, RC-QAR Hamiltonian [34, 50]

$$\begin{aligned} \hat{H}_{RC-QAR} = & \sum_{i=1}^3 \epsilon_i |i\rangle \langle i| + \sum_{\alpha=\{c,w\}} \Omega_\alpha \hat{a}_\alpha^\dagger \hat{a}_\alpha \\ & + \sum_{\alpha=\{c,w\}} \hat{S}_\alpha \lambda_\alpha (\hat{a}_\alpha^\dagger + \hat{a}_\alpha) + \sum_{\alpha=\{c,w\}} \frac{g_{\alpha,k}^2}{\omega_{\alpha,k}} (\hat{a}_\alpha^\dagger + \hat{a}_\alpha)^2 \\ & + \sum_k \nu_{h,k} \left( \hat{c}_{h,k}^\dagger + \hat{S}_h \frac{f_{h,k}}{\nu_{h,k}} \right) \left( \hat{c}_{h,k} + \hat{S}_h \frac{f_{h,k}}{\nu_{h,k}} \right) \\ & + \sum_{\alpha=\{c,w\}} (\hat{a}_\alpha^\dagger + \hat{a}_\alpha) \sum_k g_{\alpha,k} (\hat{b}_{\alpha,k}^\dagger + \hat{b}_{\alpha,k}) \\ & + \sum_k \nu_{h,k} \hat{c}_{h,k}^\dagger \hat{c}_{h,k} + \sum_{\alpha=\{c,w\};k} \omega_{\alpha,k} \hat{b}_{\alpha,k}^\dagger \hat{b}_{\alpha,k}. \end{aligned} \quad (4)$$

The first four terms constitute the *extended system* with  $\hat{a}_{c,w}^\dagger$  ( $\hat{a}_{c,w}$ ) as bosonic creation (annihilation) operators of two RCs with frequencies  $\Omega_{c,w}$ , extracted from the cold and work environments, respectively. The RCs are coupled to the 3-level system by  $\lambda_\alpha$ . Note the quadratic term in the RC, which emerges after the mapping. The third and fourth lines describe the coupling of the system to the hot bath, unaltered by the mapping, and the coupling of the RCs to the work and cold baths;  $\hat{b}_{\alpha,k}^\dagger$  ( $\hat{b}_{\alpha,k}$ ) are operators of the residual baths and  $g_{\alpha,k}$  are coupling parameters that build the spectral density functions  $J_{RC,\alpha}(\omega) = \sum_k g_{\alpha,k}^2 \delta(\omega - \omega_{\alpha,k})$ . The last line includes the Hamiltonians of the original hot bath, and the residual cold and work reservoirs.

If the spectral density function for the original cold and work baths, Eq. (1), is Brownian, Eq. (2), then the spectral density functions of the residual baths become Ohmic with an infinite high frequency cut-off,  $J_{RC,\alpha}(\omega) = \gamma_\alpha \omega e^{-|\omega|/\Lambda_\alpha}$  [34, 48]. In the RC representation,  $\gamma_\alpha$  is a dimensionless coupling constant of the RC to the residual bath—later assumed small to justify a perturbative treatment for the extended system. Furthermore,  $\Lambda_\alpha$  is the cutoff frequency of the  $\alpha$ th bath. We perform the RC mapping on the work and cold baths only. Thus, the hot bath is assumed Ohmic from the start, while the cold and work residual baths are Ohmic only after the mapping. For convenience, we assume a symmetry between the baths such that  $\Omega_c = \Omega_w = \Omega$ ,  $\lambda_c = \lambda_w = \lambda$  and  $\gamma_{c,h,w} = \gamma$ .

*Method.* Due to the assumption of weak coupling between the *extended system* and the residual baths (small  $\gamma$ ), one can employ standard perturbative quantum master equation tools to study transport behavior in the RC-QAR model, a method referred to as the RC-QME [34, 48, 49]. The procedure involves three steps. (i) We truncate the two RCs harmonic oscillators to include  $M$  levels each. Working in the occupation basis, the resulting  $3 \times M^2$ -dimension extended system's Hamiltonian is denoted by  $\hat{H}_{ES}^M$ . We note that the computational complexity of the RC-QME method rapidly increases with the dimensionality of the extended system as  $(3 \times M^2)^4$ . The value of  $M$  is decided on by converging simulations of the desired expectation value, see [54]. (ii) We diagonalize the extended system  $\hat{H}_{ES}^M \rightarrow \hat{H}_{ES}^D$ , and represent the system-bath coupling operators in the energy eigenbasis [54]. (iii) We use the Redfield equation to study steady state transport of the  $3M^2$ -dimension extended system. This amounts to the assumptions that the RC is weakly coupled to the residual environments, the dynamics is Markovian, and the initial state of the open system is a product state of the extended system and baths, the latter prepared in canonical states. Formally, the Redfield equation is given by  $\dot{\rho}_{ES}(t) = -i[\hat{H}_{ES}^D, \rho_{ES}] + \sum_\alpha \mathcal{D}_\alpha(\rho_{ES})$ . The dissipators  $\mathcal{D}_{w,h,c}(\rho_{ES})$  are additive given the weak coupling approximation of the RCs to their residual baths, but the  $w, c$  dissipators depend in a *nonadditive* manner on the original coupling parameters,  $\lambda_{w,c}$ .

We solve the Redfield equation in the energy basis under the constraint of  $\text{Tr}[\rho_{ES}(t)] = 1$  for all  $t$  and obtain the steady state density matrix of the extended system,  $\rho_{ES}^{ss}$ . The steady state heat current at the  $\alpha$  contact is  $j_\alpha = \text{Tr}[\mathcal{D}_\alpha(\rho_{ES}^{ss})\hat{H}_{ES}^D]$ ; the heat current is defined positive when flowing from the bath towards the system.

*Effective QAR model.*— Assuming that the RC frequencies are high,  $\Omega \gg \Delta, \lambda, T$  we can recreate a 3-level model for the refrigerator by truncating the extended  $3M^2$  (QAR with two RCs) system. This effective (EFF) model captures strong-coupling effects through

level renormalization, a principle introduced in Ref. [34] for the nonequilibrium spin-boson model. The lowest three energy levels of the manifold of  $\hat{H}_{ES}^D$  roughly correspond to the system occupying one of the levels  $|1\rangle$ ,  $|2\rangle$ , or  $|3\rangle$  [see Eq. (4)], while the two RCs are in their respective ground state (energy  $2 \times \frac{1}{2}\Omega$ ); the next manifold, which is further away in energy, involves a single RC excitation (energy  $\frac{1}{2}\Omega + \frac{3}{2}\Omega \gg \Delta, \lambda$ ). The effective model includes three levels, similarly to the original QAR Hamiltonian before the incorporation of the RCs, Eq. (1). However, it includes strong coupling effects through the  $\lambda$ -dependent eigenenergies and system-bath coupling matrix elements, see [54]. We study steady state transport in this model using the Redfield equation, and refer to these calculations as the EFF-QME approach.

*Results.*— What are the expected signatures of strong coupling on the performance of thermal machines? We recount: (i) *Renormalization of energy parameters*, leading to the reshaping of the performance window [34]. (ii) *Bath-cooperative transitions* [24, 33], which can lead to *leakage*, that is heat current flowing directly from the work bath to the cold one. In this situation,  $j_w > 0$  while  $j_c < 0$ . (iii) *Off-resonant transitions* that open additional transport pathways. In the present model, strong coupling opens additional cooling cycles that involve excitations of the RCs; in the weak coupling limit, only a single cycle contributes, see Fig. 1. While running a machine with multiple cycles may enhance the cooling window, it results in *internal dissipation*, with the system unable to reach the maximal Carnot efficiency [24, 36].

To discern the relative importance of these factors, we perform heat transport simulations of the strongly-coupled 3-level QAR using (i) The Born-Markov Redfield equation *after* performing the reaction coordinate transformation on the cold and work baths (RC-QME). Based on benchmarking on the spin-boson model [34], we expect this method to accurately describe strong coupling effects even at large  $\lambda$ , as long as  $\gamma$  is small and  $\Omega$  is large. (ii) The standard Born-Markov Redfield equation without performing the RC transformation (BMR-QME). This approach obviously fails to describe the correct behavior as one increases the coupling  $\lambda$ . (iii) The Born-Markov Redfield equation on the *effective* QAR model (EFF-QME). This method presents strong  $\lambda$  effects within the renormalization of energy parameters, yet missing leakage and competing cycles.

We examine the cooling current and the window of operation in Fig. 2, presented as a function of the energy splitting  $\Delta$  (see Fig. 1) and the system-bath coupling  $\lambda$ . The colored region  $\mathcal{R}_3$  in the contour plots Fig. 2 (a)-(c) corresponds to the cooling window,  $j_c > 0$ . In contrast,  $j_c < 0$  in regions  $\mathcal{R}_1$ ,  $\mathcal{R}_2$  and  $\mathcal{R}_4$  (we explain their characteristics below). Focusing on  $\mathcal{R}_3$  and comparing weak coupling, Fig. 2(a), to RC-QME calculations, Fig. 2(b), we arrive at the main conclusion of our work: Reshaping of the cooling window is a central impact of strong

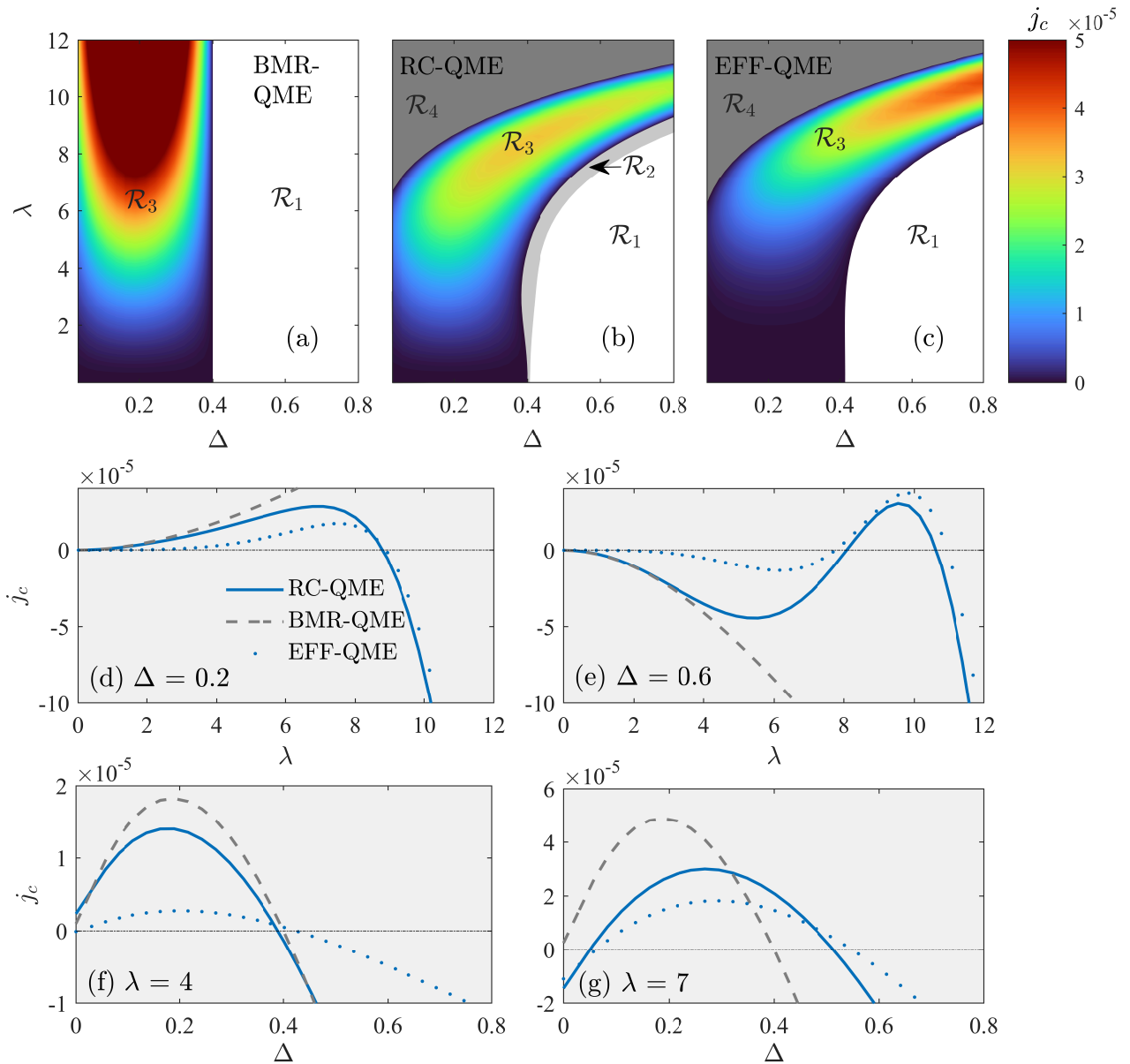


FIG. 2. (a)-(c) Contour maps of the cooling current  $j_c$  as a function of the coupling strength  $\lambda$  and energy spacing  $\epsilon_2 - \epsilon_1 = \Delta$  using the (a) BMR-QME, (b) RC-QME with  $M = 6$ , (c) EFF-QME method. The system cools ( $j_c > 0$ ) in region  $\mathcal{R}_3$  only. We further color  $\mathcal{R}_2$  and  $\mathcal{R}_4$  in which  $j_w > 0$  but  $j_c < 0$ ; in  $\mathcal{R}_1$  both  $j_w < 0$  and  $j_c < 0$ . (d)-(g) Cuts of contour maps, with  $j_c$  as a function of (d)  $\lambda$  with  $\Delta = 0.2$ , (e)  $\lambda$  with  $\Delta = 0.6$ , (f)  $\Delta$  with  $\lambda = 4$ , and (g)  $\Delta$  with  $\lambda = 7$ . We use BMR-QME (---), RC-QME with  $M = 6$  (—) and the EFF-QME (.....). Other parameters are  $\Omega = 20$ ,  $T_c = 0.25$ ,  $T_h = 0.5$ ,  $T_w = 1.5$ ,  $\gamma = 0.0071/\pi$ ,  $\Lambda_c = \Lambda_h = \Lambda_w = 500$ .

coupling, and it results from parameter renormalization at strong coupling; we show energy shift and modulation of couplings with  $\lambda$  in Ref. [54]. This observation is corroborated by noting that EFF-QME simulations in Fig. 2(c), which do not incorporate leakage and off-resonant effects, very well emulate strong coupling characteristics.

In the weak coupling limit, Fig. 2(a), the cooling window is defined by the condition  $\frac{\epsilon_2 - \epsilon_1}{\epsilon_3 - \epsilon_1} \leq \frac{\beta_h - \beta_w}{\beta_c - \beta_w}$  [35], which translates to  $\Delta \leq 0.4$  in our parameters, indepen-

dent of  $\lambda$ . In the EFF-QAR model, the relevant measure for the cooling window is the ratio  $\frac{E_2(\lambda) - E_1(\lambda)}{E_3(\lambda) - E_1(\lambda)} \leq \frac{\beta_h - \beta_w}{\beta_c - \beta_w}$ , with  $E_i(\lambda)$  as the first three eigenvalues of the extended system. Indeed, this inequality well predicts the cooling window beyond weak coupling [54]. The remarkable success of the EFF-QAR model (compare Fig. 2(c) to 2(b)) evinces that renormalization of parameters is a central fingerprint of strong system-bath coupling. The impact of heat leakage ( $j_c < 0$  but  $j_w > 0$ ) is further identified

in Fig. 2(b) by  $\mathcal{R}_2$  and  $\mathcal{R}_4$ : While within  $\mathcal{R}_2$ , ordering of levels still follows the  $\lambda = 0$  limit, in region  $\mathcal{R}_4$ , parameter-shift is significant such that the level corresponding to  $\epsilon_2$  crosses the one originating from  $\epsilon_1$ , see [54]. Finally, in region  $\mathcal{R}_1$  both  $j_w < 0$  and  $j_c < 0$ , with heat arriving from the hot bath.

The relationship between the cooling current,  $j_c$ , and the coefficient of performance (COP),  $j_c/j_w$ , is displayed in Fig. 3. In the weak coupling limit, the 3-level model can reach Carnot's bound  $\eta_C = (\beta_h - \beta_w)/(\beta_c - \beta_w)$ , albeit at a vanishing cooling power [35]. This idealized scenario is applicable only for reversible thermal machines, in the absence of heat leaks and internal dissipation. In contrast, at stronger coupling these processes become active, thus suppressing the COP. Moreover, at strong coupling the cooling current is smaller than the weak coupling value, demonstrating the negative impact of heat leaks (direct heat flow from the work to the cold bath).

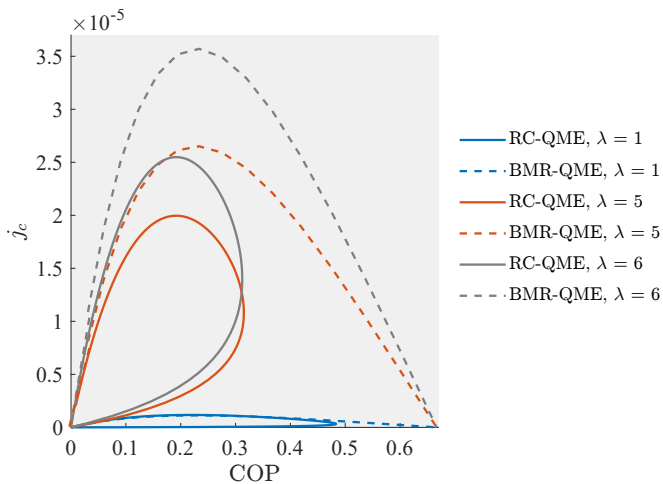


FIG. 3. Cooling current ( $j_c$ ) as a function of the coefficient of performance (COP) with the BMR-QME (dashed) and RC-QME (full) approaches at different values for  $\lambda$ . Other parameters are the same as in Fig. 2.

*Summary.* We revealed that a prominent signature of strong system-bath coupling in quantum thermal machines is the modification, or reshaping of the operational window, arising due to parameter renormalization. Focusing on the 3-level QAR, we reached this conclusion based on comprehensive simulations made possible with the non-perturbative RC-QME method. This observation, on the central role of parameter renormalization, was corroborated by the analysis of an *effective* 3-level QAR model, and it should hold for other types of spectral functions. Detrimental effects of strong couplings are due to heat leaks and internal dissipation, which reduce the cooling current and the COP. The design of quantum thermal machines that markedly benefit from strong system-bath coupling remains an open challenge.

DS acknowledges support from an NSERC Discovery

Grant and the Canada Research Chair program. The work of FI was supported by a CQIQC summer fellowship at the University of Toronto.

\* These authors contributed equally to this work

- [1] S. Vinjanampathy and J. Anders, Quantum thermodynamics, *Contemporary Physics* **57**, 545 (2016).
- [2] J. Goold, M. Huber, A. Riera, L. del Rio, and P. Skrzypczyk, The role of quantum information in thermodynamics—a topical review, *J. Phys. A: Math. Theor.*, **49**, 143001 (2016).
- [3] R. Kosloff, Quantum thermodynamics: A dynamical viewpoint, *Entropy* **15**, 2100 (2013).
- [4] H. E. D. Scovil and E. O. Schulz-DuBois, Three-Level Masers as Heat Engines, *Phys. Rev. Lett.* **2**, 262 (1959).
- [5] G. Maslennikov, S. Ding, R. Hablützel, J. Gan, A. Roulet, S. Nimmrichter, J. Dai, V. Scarani, D. Matsukevich, Quantum absorption refrigerator with trapped ions, *Nature Comm.* **10**, 202 (2019).
- [6] J. Roßnagel, S. T. Dawkins, K. N. Tolazzi, O. Abah, E. Lutz, F. Schmidt-Kaler, and K. Singer, A single-atom heat engine, *Science* **352**, 325 (2016).
- [7] D. von Lindenfels, O. Grab, C. T. Schmiegelow, V. Kaushal, J. Schultz, M. T. Mitchison, J. Goold, F. Schmidt-Kaler, and U. G. Poschinger, Spin Heat Engine Coupled to a Harmonic-Oscillator Flywheel, *Phys. Rev. Lett.* **123**, 080602 (2019).
- [8] R. Uzdin, A. Levy, and R. Kosloff, Equivalence of Quantum Heat Machines, and Quantum-Thermodynamic Signatures, *Phys. Rev. X* **5**, 031044 (2015).
- [9] A. Streltsov, G. Adesso, and M. B. Plenio Colloquium: Quantum coherence as a resource, *Rev. Mod. Phys.* **89**, 041003 (2017).
- [10] M. Kilgour and D. Segal, Coherence and decoherence in quantum absorption refrigerators, *Phys. Rev. E* **98**, 012117 (2018).
- [11] G. Francica, F. C. Binder, G. Guarnieri, M. T. Mitchison, J. Goold, and F. Plastina, Quantum Coherence and Ergotropy, *Phys. Rev. Lett.* **125**, 180603 (2020).
- [12] C.L. Latune, I. Sinayskiy, and F. Petruccione, Roles of quantum coherences in thermal machines, *The European Physical Journal Special Topics* **230**, 841 (2021).
- [13] N. Brunner, M. Huber, N. Linden, S. Popescu, R. Silva, and P. Skrzypczyk, Entanglement enhances cooling in microscopic quantum refrigerators, *Phys. Rev. E* **89**, 032115 (2014).
- [14] L. Bresque, P. A. Camati, S. Rogers, K. Murch, A. N. Jordan, and A. Auffèves, Two-Qubit Engine Fueled by Entanglement and Local Measurements, *Phys. Rev. Lett.* **126**, 120605 (2021).
- [15] C. Elouard, D. Herrera-Martí, B. Huard, and A. Auffèves, Extracting Work from Quantum Measurement in Maxwell's Demon Engines, *Phys. Rev. Lett.* **118**, 260603 (2017).
- [16] L. Buffoni, A. Solfanelli, P. Verrucchi, A. Cuccoli, and M. Campisi, Quantum Measurement Cooling, *Phys. Rev. Lett.* **122**, 070603 (2019).
- [17] N. M. Myers and S. Deffner, Thermodynamics of statistical anyons, arXiv:2102.02181
- [18] P. Strasberg, G. Schaller, N. Lambert, and T. Brandes,

- Nonequilibrium Thermodynamics in the Strong Coupling and Non-Markovian Regime Based on a Reaction Coordinate Mapping, *New J. Phys.* **18**, 073007 (2016).
- [19] A. Kato and Y. Tanimura, Quantum heat current under non-perturbative and non-Markovian conditions: Applications to heat machines, *J. Chem. Phys.* **145**, 224105 (2016).
- [20] M. Perarnau-Llobet, H. Wilming, A. Riera, R. Gallego, and J. Eisert, Strong Coupling Corrections in Quantum Thermodynamics, *Phys. Rev. Lett.* **120**, 120602 (2018).
- [21] D. Newman, F. Mintert, and A. Nazir, Performance of a Quantum Heat Engine at Strong Reservoir Coupling, *Phys. Rev. E* **95**, 032139 (2017).
- [22] A. Mu, B. K. Agarwalla, G. Schaller, and D. Segal, Qubit absorption refrigerator at strong coupling, *New J. Phys.* **19**, 123034 (2017).
- [23] W. Dou, M. A. Ochoa, A. Nitzan and J. E. Subotnik Universal approach to quantum thermodynamics in the strong coupling regime, *Phys. Rev. B* **98**, 134306 (2018).
- [24] H. M. Friedman, B. K. Agarwalla, and D. Segal, Quantum energy exchange and refrigeration: A full-counting statistics approach, *New J. Phys.* **20**, 083026 (2018).
- [25] D. Newman, F. Mintert, and A. Nazir, Quantum limit to nonequilibrium heat-engine performance imposed by strong system-reservoir coupling, *Phys. Rev. E* **101**, 052129 (2020).
- [26] C. McConnell and A. Nazir, Strong coupling in thermoelectric nanojunctions: a reaction coordinate framework, arXiv:2106.14799.
- [27] W.-M. Huang and W.-M. Zhang, Strong Coupling Quantum Thermodynamics with Renormalized Hamiltonian and Temperature, arXiv:2010.01828.
- [28] M. Wiedmann, J. T. Stockburger, and J. Ankerhold, Non-Markovian dynamics of a quantum heat engine: out-of-equilibrium operation and thermal coupling control, *New J. Phys.* **22**, 033007 (2020).
- [29] M. Brenes, J. J. Mendoza-Arenas, A. Purkayastha, M. T. Mitchison, S. R. Clark, and J. Goold, Tensor-Network Method to Simulate Strongly Interacting Quantum Thermal Machines, *Phys. Rev. X* **10**, 031040 (2020).
- [30] Y. Tanimura, Numerically “exact” approach to open quantum dynamics: The hierarchical equations of motion (HEOM), *J. Chem. Phys.* **153**, 020901 (2020).
- [31] J. Liu, K. A. Jung, and D. Segal, Periodically-driven quantum thermal machines from warming up to limit cycle, *Phys. Rev. Lett.* (2021).
- [32] N. Bergmann and M. Galperin, A Green’s function perspective on the nonequilibrium thermodynamics of open quantum systems strongly coupled to baths, *Euro. Phys. J. Special Topics* **230**, 859 (2021).
- [33] L. Nicolin and D. Segal, Non-equilibrium spin-boson model: Counting statistics and the heat exchange fluctuation theorem, *J. Chem. Phys.* **135**, 164106 (2011).
- [34] N. Anto Sztrikacs and D. Segal, Strong coupling effects in quantum thermal transport with the reaction coordinate method, *New J. Phys.* **23**, 063036 (2021).
- [35] R. Kosloff and A. Levy, Quantum Heat Engines and Refrigerators: Continuous Devices, *Ann. Rev. Phys. Chem.* **65**, 365 (2014).
- [36] L. A. Correa, J.P. Palao, and D. Alonso, Internal dissipation and heat leaks in quantum thermodynamic cycles, *Phys. Rev. E* **92**, 032136 (2015).
- [37] M. T. Mitchison, Quantum thermal absorption machines: refrigerators, engines and clocks, *Contemporary Physics* **60**, 164 (2019).
- [38] L. A. Correa, J. P. Palao, D. Alonso, and G. Adesso, Quantum-enhanced absorption refrigerators, *Sci. Rep.* **4**, 3949 (2014).
- [39] M. T. Mitchison, M. Huber, J. Prior, M. P. Woods, and M. B. Plenio, Realising a quantum absorption refrigerator with an atom-cavity system, *Quantum Sci. Technol.* **1**, 015001 (2016).
- [40] H. Friedman and D. Segal, Cooling condition for multilevel quantum absorption refrigerators, *Phys. Rev. E* **100**, 062112 (2019).
- [41] D. Segal, Current fluctuations in quantum absorption refrigerators, *Phys. Rev. E* **97**, 052145 (2018).
- [42] J. Liu and D. Segal, Coherences and the thermodynamic uncertainty relation: Insights from quantum absorption refrigerators, *Phys. Rev. E* **103**, 032138 (2021).
- [43] J. O. González, J. P. Palao, and D. Alonso, Relation between topology and heat currents in multilevel absorption machines, *New J. Phys.* **19**, 113037 (2017).
- [44] P. P. Hofer, M. Perarnau-Llobet, J. B. Brask, R. Silva, M. Huber, and N. Brunner, Autonomous quantum refrigerator in a circuit QED architecture based on a Josephson junction, *Phys. Rev. B* **94**, 235420 (2016).
- [45] K. H. Hughes, C. D. Christ, and I. Burghardt, Effective-mode representation of non-Markovian dynamics: A hierarchical approximation of the spectral density. I. Application to single surface dynamics, *J. Chem. Phys.* **131**, 024109 (2009).
- [46] K. H. Hughes, C. D. Christ, and I. Burghardt, Effective-mode representation of non-Markovian dynamics: A hierarchical approximation of the spectral density II. Application to environment-induced nonadiabatic dynamics, *J. Chem. Phys.* **131**, 124108 (2009).
- [47] R. Martinazzo, B. Vacchini, K. H. Hughes, and I. Burghardt, Universal Markovian reduction of Brownian particle dynamics, *J. Chem. Phys.* **134**, 011101 (2011).
- [48] J. Iles-Smith, N. Lambert, and A. Nazir, Environmental dynamics, correlations, and the emergence of noncanonical equilibrium states in open quantum systems, *Phys. Rev. A* **90**, 032114 (2014).
- [49] J. Iles-Smith A. G. Dijkstra, N. Lambert, and A. Nazir, Energy transfer in structured and unstructured environments: Master equations beyond the Born-Markov approximations, *J. Chem. Phys.* **144**, 044110 (2016).
- [50] A. Nazir and G. Schaller, The Reaction Coordinate Mapping in Quantum Thermodynamics, in *Thermodynamics in the Quantum Regime: Fundamental Aspects and New Directions*, Springer International Publishing, 551-577 (2018).
- [51] L.A. Correa, B. Xu, B. Morris and G. Adesso, Pushing the limits of the reaction-coordinate mapping, *J. Chem. Phys.* **151**, 094107 (2019).
- [52] P. Strasberg, G.t Schaller, T. L. Schmidt, and M. Esposito, Fermionic reaction coordinates and their application to an autonomous Maxwell demon in the strong-coupling regime, *Phys. Rev. B* **97**, 205405 (2018).
- [53] C. L. Latune, Steady state in strong bath coupling: reaction coordinate versus perturbative expansion, arXiv:2110.03169.
- [54] See Supplementary Information file.

# Supplemental Material: Strong system-bath coupling reshapes characteristics of quantum thermal machines

Felix Ivander,<sup>1,\*</sup> Nicholas Anto-Sztrikacs,<sup>2,\*</sup> and Dvira Segal<sup>1,2</sup>

<sup>1</sup>*Chemical Physics Theory Group, Department of Chemistry and Centre for Quantum Information and Quantum Control, University of Toronto, 80 Saint George St., Toronto, Ontario, M5S 3H6, Canada*

<sup>2</sup>*Department of Physics, 60 Saint George St., University of Toronto, Toronto, Ontario, Canada M5S 1A7*  
(Dated: November 10, 2021)

In this Supplemental Material, we provide additional details on the application of the reaction-coordinate (RC) mapping on the 3-level quantum absorption refrigerator (QAR) model and the computational methods used. Sec. S1 provides a top-level picture of the methods adopted in the main text. In Sec. S2, we detail steps in arriving at the reaction coordinate quantum master equation (RC-QME) framework. In Sec. S3, we justify the construction of the effective 3-level QAR model, which incorporates strong couplings with renormalized parameters only. We discuss aspects of convergence of the RC-QME method in Sec. S4. In Sec. S5, we present additional simulations of the 3-level QAR in different parameters regimes, discussing the cooling current and the coefficient of performance (COP).

## S1. DIAGRAM OF METHODS

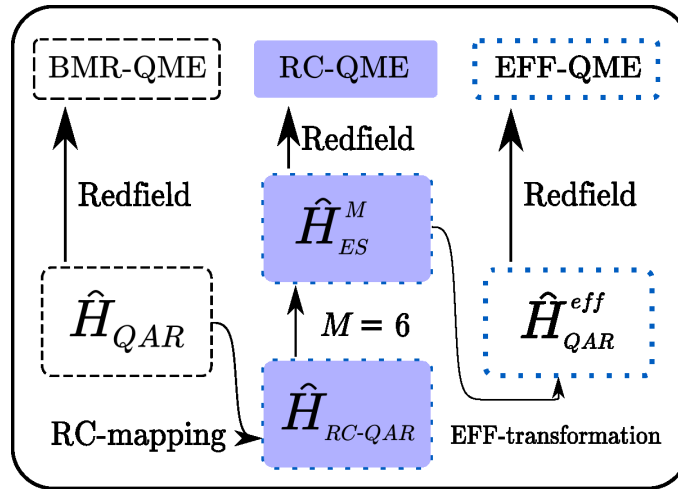


Figure S1. A schematic flowchart of methods used in this study. Objects enclosed in dashed lines (left side) concern the BMR-QME technique, where the Redfield equation is used under the weak coupling approximation. Objects in shaded blue (center) show the development of the RC-QME method (e.g., with  $M = 6$ ), a strong coupling treatment. Objects within dotted boxes (right) lead to the EFF-QME method, a truncated form of the RC-QME method.

In Fig. S1, we summarize the three approaches taken in this work:

(i) The RC-QME method allows us to uncover strong coupling effects in the performance of QARs. We start with the Hamiltonian  $\hat{H}_{QAR}$ . We use the RC mapping and incorporate two RCs into the system, thus reaching  $\hat{H}_{RC-QAR}$ . We then truncate the resulting extended model to e.g. include  $M = 6$  levels for each RC, arriving at  $\hat{H}_{ES}^M$ . We study the open dynamics of this model (in the eigenenergy representation of the extended system) using the Redfield QME.

(ii) The effective quantum master equation (EFF-QME) method approximates the RC-QME method. Here, we build an effective 3-level model from  $\hat{H}_{ES}^M$  by truncating the manifold, then proceed with the Redfield QME.

(iii) We further apply the Born-Markov-Redfield quantum master equation (BMR-QME) directly on  $\hat{H}_{QAR}$ ; this method is valid only at weak coupling.

\* These authors contributed equally to this work

## S2. THE RC-QME FRAMEWORK

We describe here the RC-QME procedure, a method non-perturbative in the system-bath coupling  $\lambda$ . The 3-level QAR Hamiltonian is manipulated in several steps before applying the Born-Markov Redfield quantum master equation. This includes the extraction of the RC coordinates, truncation of the spectrum of the RC modes, and diagonalization of the resulting extended system Hamiltonian. The starting point (see main text) is the 3-level QAR model given by the Hamiltonian

$$\hat{H}_{QAR} = \sum_{i=1}^3 \epsilon_i |i\rangle\langle i| + \sum_{\alpha=\{c,w,h\}} \sum_k \nu_{\alpha,k} \left( \hat{c}_{\alpha,k}^\dagger + \hat{S}_\alpha \frac{f_{\alpha,k}}{\nu_{\alpha,k}} \right) \left( \hat{c}_{\alpha,k} + \hat{S}_\alpha \frac{f_{\alpha,k}}{\nu_{\alpha,k}} \right). \quad (\text{S1})$$

Here,  $\epsilon_i$  denotes the  $i$ th energy level of the QAR. Without loss of generality, we set the total energy gap to be  $\epsilon_3 - \epsilon_1 = 1$  and the first energy gap as  $\epsilon_2 - \epsilon_1 = \Delta$ . The system operators  $\hat{S}_\alpha$  with  $\alpha = c, h, w$  describe the coupling of the QAR to the  $\alpha$ th bath,

$$\hat{S}_c = |1\rangle\langle 2| + h.c., \quad \hat{S}_h = |1\rangle\langle 3| + h.c., \quad \hat{S}_w = |2\rangle\langle 3| + h.c. \quad (\text{S2})$$

The baths comprise collection of harmonic modes with creation (annihilation) operators,  $\hat{c}_{\alpha,k}^\dagger$  ( $\hat{c}_{\alpha,k}$ ), and the system-bath couplings are captured by the spectral density function,  $J_\alpha(\omega) = \sum_k f_{\alpha,k}^2 \delta(\omega - \nu_{\alpha,k})$ , with real-valued  $f_{\alpha,k}$  the coupling energy between the QAR and a bath mode of frequency  $\nu_{\alpha,k}$ .

### A. RC mapping

To handle strong coupling effects between the system (3-level model) and the cold and work baths, we invoke the reaction coordinate mapping for those reservoirs. This results in the following RC-QAR Hamiltonian

$$\begin{aligned} \hat{H}_{RC-QAR} = & \sum_{i=1}^3 \epsilon_i |i\rangle\langle i| + \sum_{\alpha=\{c,w\}} \Omega_\alpha \hat{a}_\alpha^\dagger \hat{a}_\alpha + \sum_{\alpha=\{c,w\}} \hat{S}_\alpha \lambda_\alpha (\hat{a}_\alpha^\dagger + \hat{a}_\alpha) + \sum_{\alpha=\{c,w\}} \frac{g_{\alpha,k}^2}{\omega_{\alpha,k}} (\hat{a}_\alpha^\dagger + \hat{a}_\alpha)^2 \\ & + \sum_k \nu_{h,k} \left( \hat{c}_{h,k}^\dagger + \hat{S}_h \frac{f_{h,k}}{\nu_{h,k}} \right) \left( \hat{c}_{h,k} + \hat{S}_h \frac{f_{h,k}}{\nu_{h,k}} \right) + \sum_{\alpha=\{c,w\}} (\hat{a}_\alpha^\dagger + \hat{a}_\alpha) \sum_k g_{\alpha,k} (\hat{b}_{\alpha,k}^\dagger + \hat{b}_{\alpha,k}) \\ & + \sum_k \nu_{h,k} \hat{c}_{h,k}^\dagger \hat{c}_{h,k} + \sum_{\alpha=\{c,w\};k} \omega_{\alpha,k} \hat{b}_{\alpha,k}^\dagger \hat{b}_{\alpha,k}. \end{aligned} \quad (\text{S3})$$

This mapping was reviewed in Ref. [1]. It was described in details for the related spin-boson Hamiltonian in Refs. [2, 3], and we do not repeat those steps here.

As outlined in the main text, this model now describes a QAR coupled via  $\lambda_{c,w}$  to two reaction coordinates of frequencies  $\Omega_{c,w}$  denoted by the bosonic creation (annihilation) operators  $\hat{a}_{c,w}^\dagger$  ( $\hat{a}_{c,w}$ ) extracted from the cold and work baths respectively. These reaction coordinates couple to residual cold and work baths described by the operators  $\hat{b}_{\alpha,k}^\dagger$  ( $\hat{b}_{\alpha,k}$ ). The Hamiltonian Eq. (S3) also contains the unaltered hot bath and its coupling to the QAR. The last term in the first line of Eq. (S3) is quadratic in the RC operators. In what follows, we neglect this term as it was shown to be partially eliminated from the Markovian quantum master equation [2, 3]. In the RC representation, the spectral density functions describing the interaction between the baths and the system are Ohmic,  $J_\alpha(\omega) = \gamma_\alpha \omega e^{-|\omega|/\Lambda_\alpha}$  for all baths. Here,  $\Lambda_\alpha$  is the high-frequency cutoff of the  $\alpha$ th bath.  $\gamma_\alpha$  are dimensionless coupling constants between the extended system (ES), which comprises the original three levels and the two RCs, and the baths. In what follows, these constants are assumed small to justify employing the Redfield quantum master equation technique on the extended (three levels and two RCs) system.

### B. RC truncation

In order to employ the Redfield quantum master equation on the extended system, we truncate the RC manifolds, reducing them to their first  $M$  levels. This results in a  $3 \times M^2$  dimension Hamiltonian of the extended system,  $\hat{H}_{ES}^M$ . The total Hamiltonian includes the truncated system along with the three thermal baths and the interactions between them,

$$\hat{H}_{RC-QAR}^M = \hat{H}_{ES}^M + \hat{H}_B + \hat{H}_{ES,B}^M. \quad (\text{S4})$$

Explicitly,

$$\hat{H}_{ES}^M = \sum_{i=1}^3 \epsilon_i |i\rangle\langle i| + \sum_{\alpha=\{c,w\}} \sum_{l_\alpha=0}^{M-1} \Omega_\alpha \left( l_\alpha + \frac{1}{2} \right) |l_\alpha\rangle\langle l_\alpha| + \sum_{\alpha=\{c,w\}} \lambda_\alpha \hat{S}_\alpha \sum_{l_\alpha=1}^{M-1} \sqrt{l_\alpha} |l_\alpha\rangle\langle l_\alpha - 1| + h.c. \quad (\text{S5})$$

with  $|l_\alpha\rangle$  the eigenstates of the  $\alpha$  harmonic RC mode. The baths Hamiltonian is given by

$$\hat{H}_B = \sum_{\alpha=\{c,w\}} \sum_k \omega_{\alpha,k} \hat{b}_{\alpha,k}^\dagger \hat{b}_{\alpha,k} + \sum_k \nu_{h,k} \hat{c}_{h,k}^\dagger \hat{c}_{h,k}, \quad (\text{S6})$$



and the interaction term can be formally represented as

$$\hat{H}_{ES,B}^M = \sum_{\alpha=\{c,w,h\}} \hat{V}_{ES,\alpha}^M \otimes \hat{B}_\alpha. \quad (\text{S7})$$

In this expression,  $\alpha$  goes over the three heat baths—albeit with the hot bath showing a coupling form distinct from the cold and work baths, since it did not undergo the RC mapping,

$$\begin{aligned} \hat{V}_{ES,\alpha}^M &= \sum_{l_\alpha=1}^{M-1} \sqrt{l_\alpha} (|l_\alpha\rangle\langle l_\alpha-1| + |l_\alpha-1\rangle\langle l_\alpha|), \quad \hat{B}_\alpha = \sum_k g_{\alpha,k} (\hat{b}_{\alpha,k}^\dagger + \hat{b}_{\alpha,k}), \quad \text{for } \alpha = w, c \\ \hat{V}_{ES,h}^M &= \hat{S}_h, \quad \hat{B}_h = \sum_k f_{h,k} (\hat{c}_{h,k}^\dagger + \hat{c}_{h,k}). \end{aligned} \quad (\text{S8})$$

### C. Diagonalization of the extended system

In order to study dynamics and transport with the Redfield quantum master equation, we diagonalize the truncated-extended system Hamiltonian, Eq. (S5). This step is typically done numerically. The diagonalization involves the unitary operator  $\hat{U}$ ,

$$\hat{H}_{ES}^D = \hat{U}^\dagger \hat{H}_{ES}^M \hat{U}, \quad \hat{V}_{ES,\alpha}^D = \hat{U}^\dagger \hat{V}_{ES,\alpha}^M \hat{U}. \quad (\text{S9})$$

We denote the eigenenergies of  $\hat{H}_{ES}^M$  by  $E_n(\vec{\lambda})$ ;  $n = 1, 2, \dots, 3M^2$ , and present the first six of them in Fig. S2. Additionally, in Fig. S3 we display the system-bath coupling in the energy eigenbasis. As an example, we display several matrix elements,  $|\langle m(\vec{\lambda}) | \hat{V}_{ES,\alpha=w}^D | n(\vec{\lambda}) \rangle|$  with  $|n(\vec{\lambda})\rangle$  and  $|m(\vec{\lambda})\rangle$  eigenvectors of  $\hat{H}_{ES}^M$ ; we group the coupling parameters  $\lambda_\alpha$  with a vector notation  $\vec{\lambda} = (\lambda_c, \lambda_w)$ .

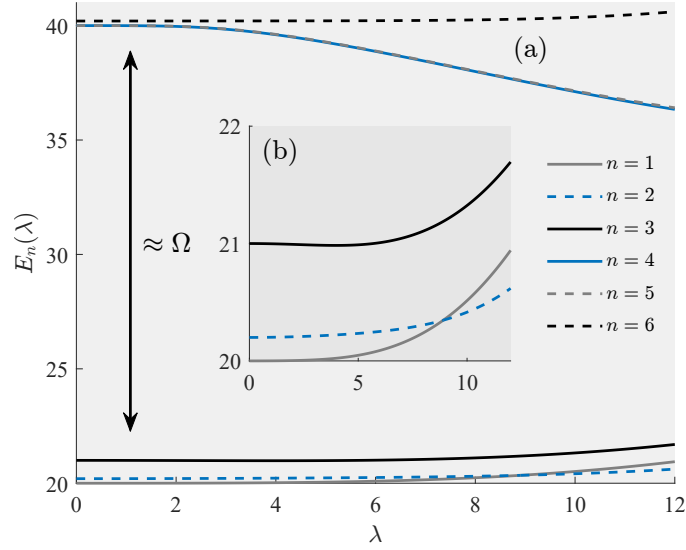


Figure S2. (a) The first 6 eigenenergies of the extended system Hamiltonian  $\hat{H}_{ES}^M$ , Eq. (S5). (b) The first 3 eigenenergies zoomed for clarity. Parameters are  $\epsilon_1 = 0$ ;  $\epsilon_2 = \Delta = 0.2$ ,  $\epsilon_3 = 1$  and RCs with  $\Omega = 20$  and  $M = 6$  levels.

### D. Redfield equation

The Redfield quantum master equation for the dynamics of the extended system density matrix,  $\rho_{ES}$ , can be written in the Schrödinger picture as [4]

$$\begin{aligned} \dot{\rho}_{ES,mn}(t) &= -i\omega_{mn}\rho_{ES,mn}(t) \\ &+ \sum_\alpha \sum_{j,k} [R_{mj,jk}^\alpha(\omega_{kj})\rho_{ES,kn}(t) + R_{nk,kj}^{\alpha*}(\omega_{jk})\rho_{ES,mj}(t) \\ &- R_{kn,mj}^\alpha(\omega_{jm})\rho_{ES,jk}(t) - R_{jn,mk}^{\alpha*}(\omega_{kn})\rho_{ES,jk}(t)]. \end{aligned} \quad (\text{S10})$$

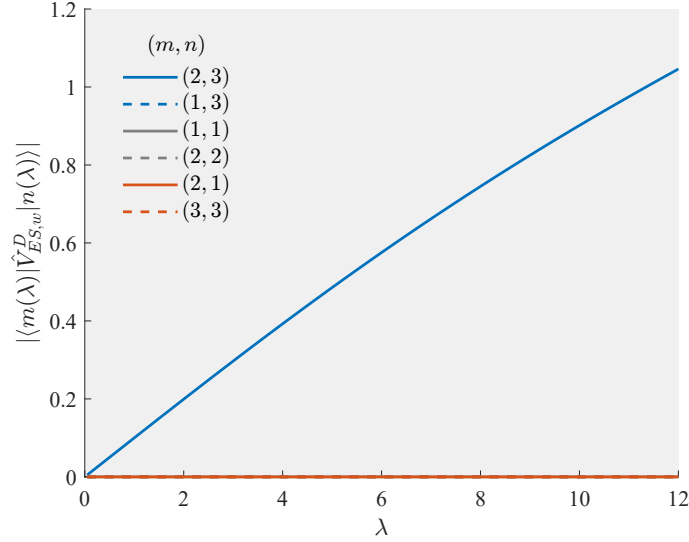


Figure S3. Magnitudes of matrix elements of  $\hat{V}_{ES,w}^D$  with  $M = 6$ . Here  $|m(\vec{\lambda})\rangle$  and  $|n(\vec{\lambda})\rangle$  are eigenvectors of  $\hat{H}_{ES}^M$ . In the present parameters—for very large  $\Omega$ —the work bath dominantly couples to a single transition, between the second and third eigenstates, while the other transitions are close to zero. Parameters are identical to Fig. S2.

Here,  $\omega_{mn} = E_m(\vec{\lambda}) - E_n(\vec{\lambda})$  are the eigenenergies of the extended system. The elements of the  $R$  super-operator are given by half Fourier transform of bath autocorrelation functions [4],

$$\begin{aligned} R_{mn,jk}^\alpha(\omega) &= (V_{ES,\alpha}^D)_{m,n} (V_{ES,\alpha}^D)_{j,k} \int_0^\infty d\tau e^{i\omega\tau} \langle B_\alpha(\tau) B_\alpha \rangle \\ &= (V_{ES,\alpha}^D)_{m,n} (V_{ES,\alpha}^D)_{j,k} [\Gamma_\alpha(\omega) + i\Delta_\alpha(\omega)]. \end{aligned} \quad (\text{S11})$$

These autocorrelation functions are evaluated with respect to the thermal state of their respective baths. In what follows, we neglect the imaginary component of the dissipators,  $\Delta_\alpha$ , as it can be shown that they cancel out the quadratic term in the RC Hamiltonian, Eq. (S3) [2]. For harmonic environments and a bilinear coupling between the extended system and the residual environments, the real part of the  $R$  tensor reduces to

$$\Gamma_\alpha(\omega) = \begin{cases} \pi J_\alpha(\omega) n_\alpha(\omega) & \omega > 0 \\ \pi J_\alpha(|\omega|) [(n_\alpha(|\omega|) + 1)] & \omega < 0. \\ \pi \gamma_\alpha / \beta_\alpha & \omega = 0 \end{cases} \quad (\text{S12})$$

$n_\alpha(\omega)$  is the Bose-Einstein distribution function of the  $\alpha$ th bath at inverse temperature  $\beta_\alpha$ ;  $J_\alpha(\omega)$  is the spectral function of bath  $\alpha$ . In the RC-QME method as described here, these functions are all ohmic.

To calculate heat currents flowing through the system, we write down the Redfield equation as

$$\dot{\rho}_{ES}(t) = -i[\hat{H}_{ES}^D, \rho_{ES}] + \mathcal{D}_w(\rho_{ES}) + \mathcal{D}_h(\rho_{ES}) + \mathcal{D}_c(\rho_{ES}), \quad (\text{S13})$$

with the dissipators  $\mathcal{D}_{w,h,c}(\rho_{ES})$  prepared based on Eq. (S10). These dissipators are additive given the weak coupling approximation of the RCs to their residual baths. However, the dissipators  $\mathcal{D}_{\alpha=w,c}$  depend in a non-additive way on the original coupling parameters,  $\lambda_{w,c}$ . We solve this equation in steady state to obtain the long time solution,  $\rho_{ES}^{ss}$ . The steady state heat current at the  $\alpha$  contact is  $j_\alpha = \text{Tr}[\mathcal{D}_\alpha(\rho_{ES}^{ss}) \hat{H}_{ES}^D]$ .

### S3. EFFECTIVE QUANTUM ABSORPTION REFRIGERATOR MODEL

A powerful aspect of the RC mapping as described in Sec. S2 is that it allows the construction of an effective low-dimension QAR model (EFF-QAR), which takes into account strong coupling effects in the shift (renormalization) of parameters relative to the weak-coupling limit. This effective model is applicable when  $\Omega_\alpha$  is large ( $\Omega_\alpha \gg \lambda_\alpha, T_\alpha, \Delta$ ). In this regime, dynamics is determined to a large extent by the lowest 3 eigenstates of  $\hat{H}_{ES}^M$  since excitations of the RC oscillators beyond their ground state are small. The effective model is constructed as follows. Once the diagonalization is performed in Eq. (S9) on a large enough  $M$  (where convergence is achieved), we take into account only the three lowest eigenstates of the extended system (S5) and write

down the effective QAR Hamiltonian as

$$\begin{aligned} \hat{H}_{QAR}^{eff} = & \sum_{n=1}^3 E_n(\vec{\lambda}) |n(\vec{\lambda})\rangle \langle n(\vec{\lambda})| + \sum_{\alpha} F_{\alpha}(\vec{\lambda}) \hat{S}_{\alpha} \sum_k g_{\alpha,k} (\hat{b}_{\alpha,k}^{\dagger} + \hat{b}_{\alpha,k}) + \hat{S}_h \sum_k f_{h,k} (\hat{c}_{h,k}^{\dagger} + \hat{c}_{h,k}) \\ & + \sum_{\alpha,k} \omega_{\alpha,k} \hat{b}_{\alpha,k}^{\dagger} \hat{b}_{\alpha,k} + \sum_k \nu_{h,k} \hat{c}_{h,k}^{\dagger} \hat{c}_{h,k}. \end{aligned} \quad (\text{S14})$$

The energy levels of the QAR are  $E_1(\vec{\lambda})$ ,  $E_2(\vec{\lambda})$  and  $E_3(\vec{\lambda})$ , which should be compared to  $\epsilon_1$ ,  $\epsilon_2$ ,  $\epsilon_3$ , respectively, the latter the levels in the original QAR picture. The eigenvectors associated with the energy levels  $E_n(\vec{\lambda})$  are  $|n(\vec{\lambda})\rangle$ . The dimensionless real-valued factors  $F_{\alpha}(\vec{\lambda})$  that decorate the system-bath coupling operators for the work and cold baths are  $F_c(\vec{\lambda}) = \langle 1(\vec{\lambda}) | \hat{V}_{ES,c}^M | 2(\vec{\lambda}) \rangle$  and  $F_w(\vec{\lambda}) = \langle 2(\vec{\lambda}) | \hat{V}_{ES,w}^M | 3(\vec{\lambda}) \rangle$ . We can then define a new spectral density function for the cold and work baths, scaled by  $F_{\alpha}(\vec{\lambda})$ ,

$$J_{QAR,\alpha}^{eff}(\omega) = \gamma_{\alpha} \omega [F_{\alpha}(\vec{\lambda})]^2 e^{-|\omega|/\Lambda_{\alpha}} \quad (\text{S15})$$

For notation convenience, in what follows we suppress the vector notation on  $\vec{\lambda}$  and use identical RC parameters for the  $w$  and  $c$  baths,  $\Omega_{\alpha} = \Omega$ ,  $\lambda_{\alpha} = \lambda$ , as well as  $\gamma_{\alpha} = \gamma$  for  $\alpha = h, w, c$ . We now make several remarks pertaining to the effective QAR Hamiltonian Eq. (S14):

(i) The Effective QAR model is justified in Figs. S2 and S3. First, in Fig. S2 we show the 6 lowest eigenenergies of the extended system Hamiltonian for  $M = 6$ , [Eq. (S5)], presented as a function of the coupling strength  $\lambda$ . There is an energy separation of order  $\Omega$  between the lowest three levels (corresponding to the ground levels of the two RCs while the QAR is free to occupy any one of its three levels), and the next manifold of excited states. Moreover, Fig. S3 shows that the work bath, for example, mainly induces the transition between the states  $|2(\lambda)\rangle$  and  $|3(\lambda)\rangle$ , in correspondence with the original QAR model. Similarly (not shown), the cold bath mainly induces the transition between the states  $|1(\lambda)\rangle$  and  $|2(\lambda)\rangle$ , again in correspondence with the original QAR model.

(ii) Simulating transport characteristics with the EFF-QME is cheap and intuitive. We use the standard Redfield quantum master equation. This calculation is identical to what is being done at weak coupling with the original QAR model of Eq. (S1); in the effective model, energies and coupling parameters implicitly depend on  $\lambda$ .

(iii) The cooling performance of the effective QAR model can be readily obtained by repeating standard derivations as in Ref. [5] (see also Appendix B in Ref. [6]). Significantly, once building the effective model one does not need to perform any dynamical simulations to identify the cooling window of the QAR in the strong coupling regime: Using the Redfield quantum master equation, we write the cooling condition as

$$\frac{E_2(\lambda) - E_1(\lambda)}{E_3(\lambda) - E_1(\lambda)} \leq \frac{\beta_h - \beta_w}{\beta_c - \beta_w}, \quad (\text{S16})$$

which is analogous to the weak coupling result. We demonstrate this point in Fig. S4. In the presented parameters,  $\frac{\beta_h - \beta_w}{\beta_c - \beta_w} = 0.4$ , which defines the cooling region. We observe that for  $\Delta = 0.6$ , the system enters the cooling region at  $\lambda \approx 8$ , but leaves it at a stronger coupling when  $\lambda \approx 11$  (see also Fig. 2(b) in the main text). In contrast, at smaller value,  $\Delta = 0.2$ , the system cools at weak-intermediate coupling, then stops cooling when  $\lambda \approx 9$ . This modification of the cooling condition with  $\lambda$  corresponds to the reshaping of the cooling window due to the renormalization of the energy levels with  $\lambda$ , as observed in Fig. 2 of the main text. It should be noted that one can reach extreme situations when levels cross,  $E_1(\lambda) > E_2(\lambda)$ , see Fig. S2. In this case (region  $\mathcal{R}_4$  in Fig. 2(b) of the main text), the machine no longer functions as a QAR.

(iv) Failure of the EFF-QME approach to mimic the full RC-QME behavior allows us to pinpoint strong coupling effects beyond parameter renormalization, specifically, the onset of heat leaks (heat transfer from the work bath towards the cold one). We discuss heat leaks in Sec. S5B.

#### S4. CONVERGENCE OF RC-QME SIMULATIONS

To describe the transport properties of QARs at strong coupling based on the RC-QME method, we truncate the reaction coordinate spectrum to include only the  $M$  lowest levels from the harmonic oscillator manifold, see Sec. S3 and Eq. (S5). The number of levels required to reach convergence depends on the relative magnitudes of the RC frequency  $\Omega$ , the temperature of the environment  $T_{\alpha}$  and the coupling strengths  $\lambda$ . To converge,  $M$  should be large enough such that the probability of exciting the RC oscillators to that level is sufficiently small, thus of insignificant contribution to transport.

In the main text, we utilized  $M = 6$  levels (unless otherwise stated). In Fig. S5(a) we show that results were converged with  $M$  already for  $M = 4$  when  $\Omega = 20$ . In contrast, for RCs with smaller  $\Omega$ , Fig. S5(b) shows satisfying convergence only at  $M = 7$  once  $\lambda > 10$ .

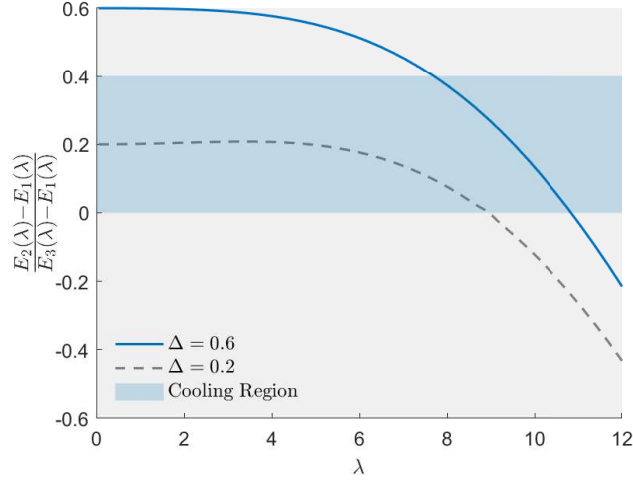


Figure S4.  $\frac{E_2(\lambda) - E_1(\lambda)}{E_3(\lambda) - E_1(\lambda)}$  as a function of  $\lambda$ , illustrating the effects of parameter renormalization on the shape of the cooling window. The region satisfying this condition is shaded in blue. In this figure,  $\Delta = 0.6$  (—) and  $\Delta = 0.2$  (---), all other parameters are identical to Fig. S2 with  $T_c = 0.25$ ,  $T_h = 0.5$ ,  $T_w = 1.5$ .

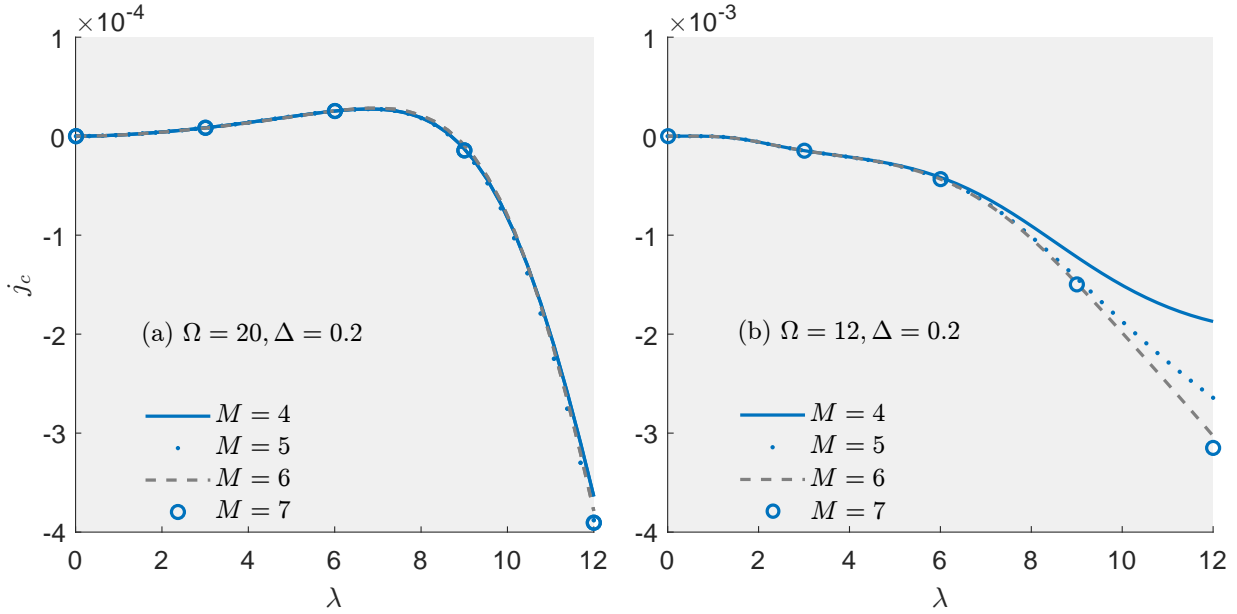


Figure S5. Cooling current  $j_c$  as a function of  $\lambda$  truncating the RCs at  $M = 4$  (—),  $M = 5$  (⋯),  $M = 6$  (---) and  $M = 7$  (hollow circles) with (a)  $\Omega = 20$ , (b)  $\Omega = 12$ . Other parameters are  $\gamma = 0.0071/\pi$ ,  $\Lambda_c = \Lambda_h = \Lambda_w = 500$ ,  $T_c = 0.25$ ,  $T_h = 0.5$ ,  $T_w = 1.5$ .

## S5. ADDITIONAL SIMULATIONS

### A. Coefficient of performance

We present additional simulations of the coefficient of performance (COP) for the QAR,  $\text{COP} \equiv \frac{j_c}{j_w}$ , in the strong coupling regime. Fig. S6 displays the COP from the nonperturbative RC-QME method, compared to the BMR-QME technique that is valid only at weak system-reservoir coupling, and the EFF-QME approach.

If the system is able to cool at weak coupling, we find that strong coupling is typically detrimental to the performance of the QAR, see Fig. S6(a)-(b) where the COP is typically suppressed with increasing  $\lambda$ . Note that in Fig. S6(a) when there is a small enhancement of the COP for intermediate  $\lambda$ , the actual cooling current is very small since  $\Delta$  is small. In contrast, in Fig. S6(c) the BMR-QME method does not predict any cooling. Here, as we increase  $\lambda$  the RC-QME method reveals that we enter the

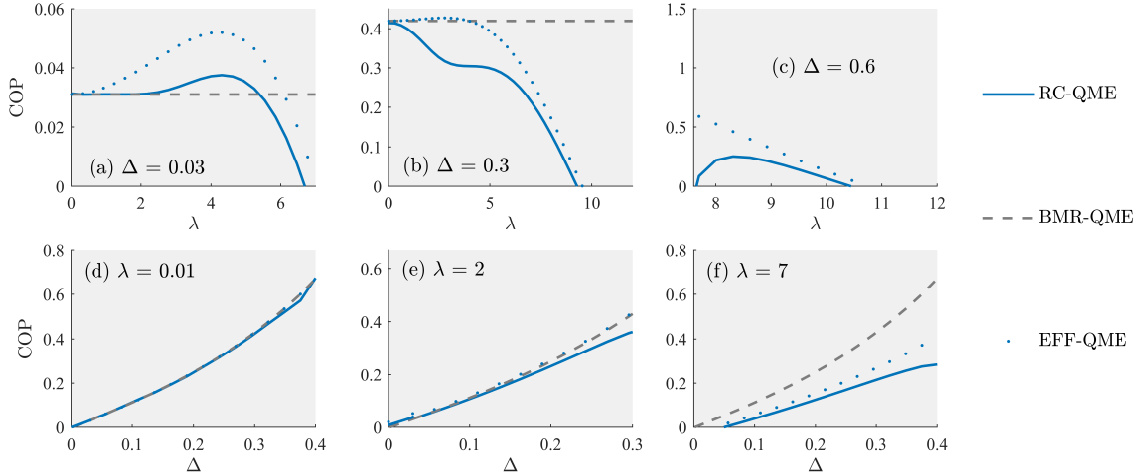


Figure S6. Coefficient of performance (COP) as a function of (a)  $\lambda$  with  $\Delta = 0.03$ , (b)  $\lambda$  with  $\Delta = 0.3$ , (c)  $\lambda$  with  $\Delta = 0.6$ , (d)  $\Delta$  with  $\lambda = 0.01$ , (e)  $\Delta$  with  $\lambda = 2$ , and (f)  $\Delta$  with  $\lambda = 7$ . Calculations were done with the RC-QME (—), the BMR-QME (---) and the EFF-QME (· · · · ·). Parameters in this plot are identical to Fig. S5 with  $\Omega = 20$ ,  $M = 6$ .

cooling window with a finite COP, increasing it until a certain threshold where it starts to be suppressed. Fig. S6(d)-(f) show that as we increase  $\Delta$  for a given coupling strength, we monotonically enhance the COP.

Fig. S6(a)-(f) demonstrate that the COP as calculated via the EFF-QME method overestimates the RC-QME technique, though it captures central trends with  $\lambda$  and  $\Delta$ . This is to be expected since the EFF-QME method does not take into account the detrimental roles of inter-bath heat flow and internal dissipation, both contributing to reduce the COP for the RC-QME.

## B. Inter-bath (leakage) heat transport

So far, we discussed the role of parameter renormalization as a central aspect of strong system-bath coupling in QARs. This aspect was rationalized with the effective description, Eq. (S14), valid if  $\Omega$ , the frequency of the reaction coordinate was made large compared to the temperature of the baths and  $\lambda$ . Since in the effective 3-level QAR description only parameter renormalizations is captured, deviations of its predictions from the RC-QME, as observed in Fig. S6, are to be associated with additional strong coupling mechanisms.

Indeed, another novel impact of strong system bath coupling is the opening of a direct heat flow pathway from the work bath towards the cold one. In this process, an excited RC from the work bath transfers its energy to the RC of the cold bath, even with little change to the population of the QAR levels. In Fig. S7 we show that by tuning  $\Omega$ , we control the extent of such a direct inter-bath transport pathway. To understand these results, we label four distinct regions in the contour plot:

In region  $\mathcal{R}_3$ ,  $j_c > 0$  and  $j_w > 0$ , and we are thus in the cooling window with heat extracted from the cold bath, assisted by the work bath, and dumped into the hot one. In regions  $\mathcal{R}_2$  and  $\mathcal{R}_4$ , we do not observe cooling as  $j_c < 0$ . Notably,  $j_w > 0$  in these regions thus heat flows from the work bath into the cold one. This direct heat flow from the work bath to the cold one, which cannot take place at weak coupling in the 3-level QAR model, is referred to as inter-bath heat transport, and it is responsible of heat leaks in the present case. We distinguish between  $\mathcal{R}_2$  and  $\mathcal{R}_4$  below. The system does not cool in  $\mathcal{R}_1$  with both  $j_c < 0$  and  $j_w < 0$ , signifying that heat flows from the hot bath towards the other two reservoirs.

We now discuss Fig. S7. First, in panel (a)  $\Omega$  is relatively small ( $\Omega = 12$ ) and inter-bath leakage is a primary effect of strong coupling: The cooling window is severely decreased due to inter-bath transport effects. In Figure S7(b), we display the same results as in Fig. 2(b) from the main text. In this case of  $\Omega = 20$ , we clearly observe four different regions:  $\mathcal{R}_3$  is the cooling window, which is significantly broader than the cooling window found in Fig. S7(a). Region  $\mathcal{R}_1$  corresponds to the “regular” no-cooling zone observed in the weak coupling limit. Next,  $\mathcal{R}_2$  illustrates where the effect of inter-bath transport takes over, resulting in a smaller cooling window. Finally,  $\mathcal{R}_4$  represents a region where there is no cooling due to the breakdown of the “correct” level scheme of the QAR (see Fig. S2); in this region,  $E_2(\lambda) < E_1(\lambda)$ , and so we are outside the cooling window.

Fig. S7(c) depicts the case of even larger RC frequency,  $\Omega = 30$ , such that excited states of the RC are negligibly populated. As a result, direct inter-bath transitions do not contribute and region  $\mathcal{R}_2$  is absent from the plot.

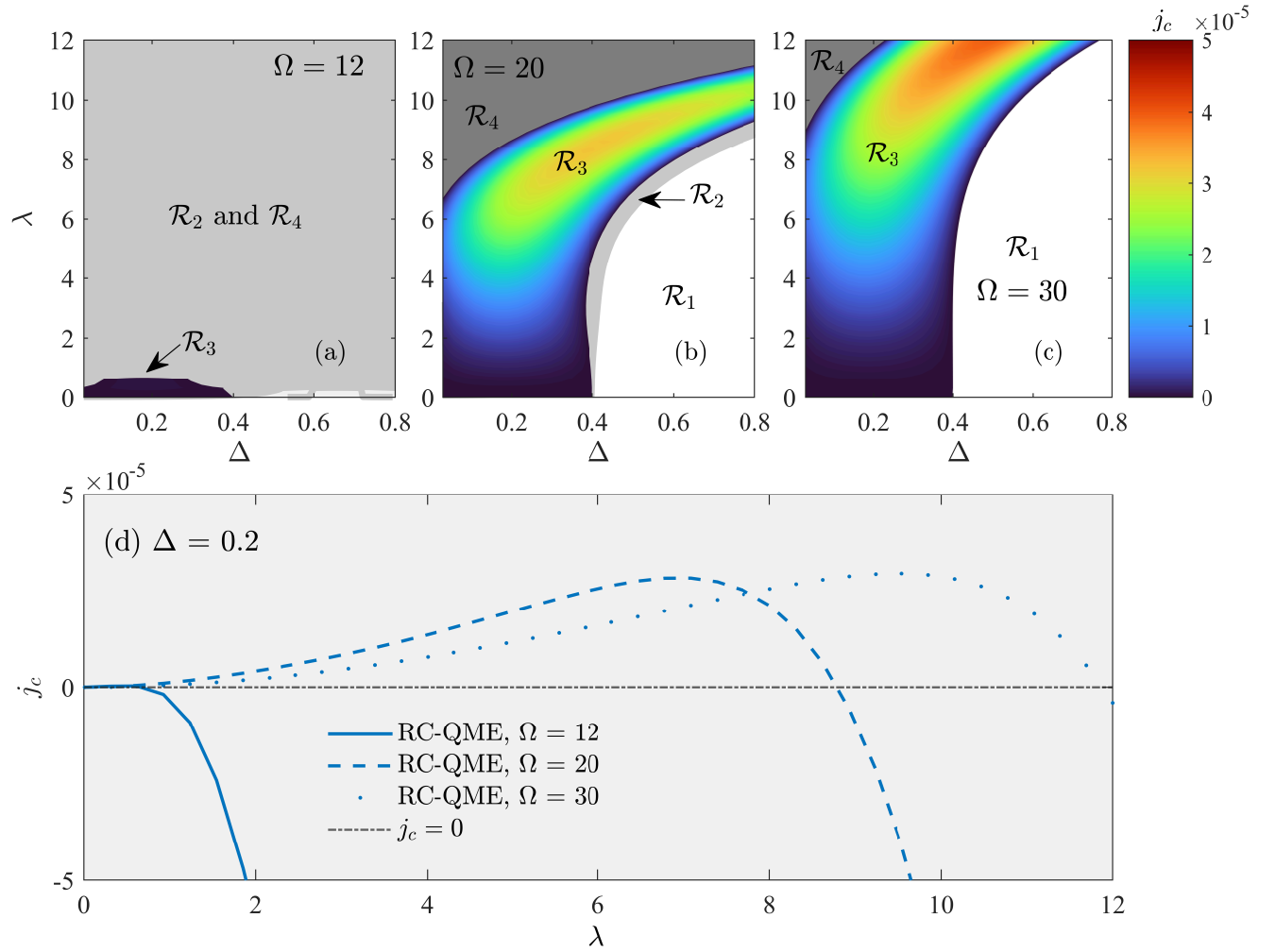


Figure S7. (a)-(c) Contour maps of the cooling current  $j_c$  as a function of the coupling strength  $\lambda$  and the energy gap  $\Delta$  using the the RC-QME method with  $M = 6$  for (a)  $\Omega = 12$ , (b)  $\Omega = 20$ , (c)  $\Omega = 30$ . (d) We present slices of the contour maps,  $j_c$  as a function of  $\lambda$  with at  $\Delta = 0.2$ , and  $\Omega = 20$  (dashed),  $\Omega = 12$  (full),  $\Omega = 30$  (dotted). Other parameters are the same as in Fig. S5.

- 
- [1] A. Nazir and G. Schaller, The Reaction Coordinate Mapping in Quantum Thermodynamics, in *Thermodynamics in the Quantum Regime: Fundamental Aspects and New Directions*, Springer International Publishing, 551-577 (2018).
- [2] J. Iles-Smith, N. Lambert, and A. Nazir, Environmental dynamics, correlations, and the emergence of noncanonical equilibrium states in open quantum systems, *Phys. Rev. A* **90**, 032114 (2014).
- [3] N. Anto Sztrikacs and D. Segal, Strong coupling effects in quantum thermal transport with the reaction coordinate method, *New J. Phys.* **23**, 063036 (2021).
- [4] Nitzan A 2006 *Chemical Dynamics in Condensed Phases: Relaxation, Transfer, and Reactions in Condensed Molecular Systems* (New York: Oxford University Press)
- [5] L. A. Correa, J. P. Palao, D. Alonso, and G. Adesso, Quantum-enhanced absorption refrigerators, *Sci. Rep.* **4**, 3949 (2014).
- [6] M. Kilgour and D. Segal, Coherence and decoherence in quantum absorption refrigerators, *Phys. Rev. E* **98**, 012117 (2018).